# Supplementary Information for: " 1D cuprates $ACuO_2$ (A=Li, Na, K, Ru, Cs): not a simple atomic insulator"

Bing Liu,[1,*] Xiaole Qiu,[1] Hongchao Yang,[1] Lianzhen Cao,[1] and Zhao Liu[2,3,†]

[1] *School of Physics and Electronic Information, Weifang University, Weifang, Shandong 261061, China*
[2] *Department of Materials Science and Engineering, Monash University, Victoria 3800, Australia*
[3] *ARC Centre of Excellent in Future Low-Energy Electronics Technologies, Monash University, Victoria 3800, Australia*

## A. Orbital interaction diagram

In this section, more details about orbital interaction diagram are discussed. To begin with, we take the linear combination of orbitals at the same WP to form SACOs according to symmetry. For example, since $d_{xy}$ share WP $1a$, there is only one $d_{xy}$ in the unit cell and the corresponding SACO at Γ point is shown in Fig. S1(a), which has $B_{1g}$ symmetry. For $p_{x,y}$, there are two equivalent positions in WP $2b$: $2b_1$ and $2b_2$. So we need to combine them first, and $\frac{|p_{x,2b_1}>+|p_{x,2b_2}>}{\sqrt{2}}$ is plotted in Fig. S1(b), $\frac{-|p_{x,2b_1}>+|p_{x,2b_2}>}{\sqrt{2}}$ in Fig. S1(c), $\frac{|p_{y,2b_1}>+|p_{y,2b_2}>}{\sqrt{2}}$ in Fig. S1(d) and $\frac{-|p_{y,2b_1}>+|p_{y,2b_2}>}{\sqrt{2}}$ in Fig. S1(e). These $p$ SACOs can then be labelled according to their symmetry. Here we take Fig. S1(e) for example. Obviously Fig. S1(e) satisfies the same transformation rule as Fig. S1(a), therefore Fig. S1(e) has symmetry $B_{1g}$. From Fig. S1(b)-(e), the energies of these $p$ SACOs can also be largely ordered. Since $B_{1g}$ $p$ SACOs are of anti-bonding nature along both x (non-periodic direction) and y (periodic direction), it must have the highest energy among all the $p$ SACOs, as indicated in Fig. S1(f). The same can be done at $X$ point. The only difference is that $B_{1g}$ $p$ SACOs are formed by $p_x$ rather than $p_y$ orbitals.

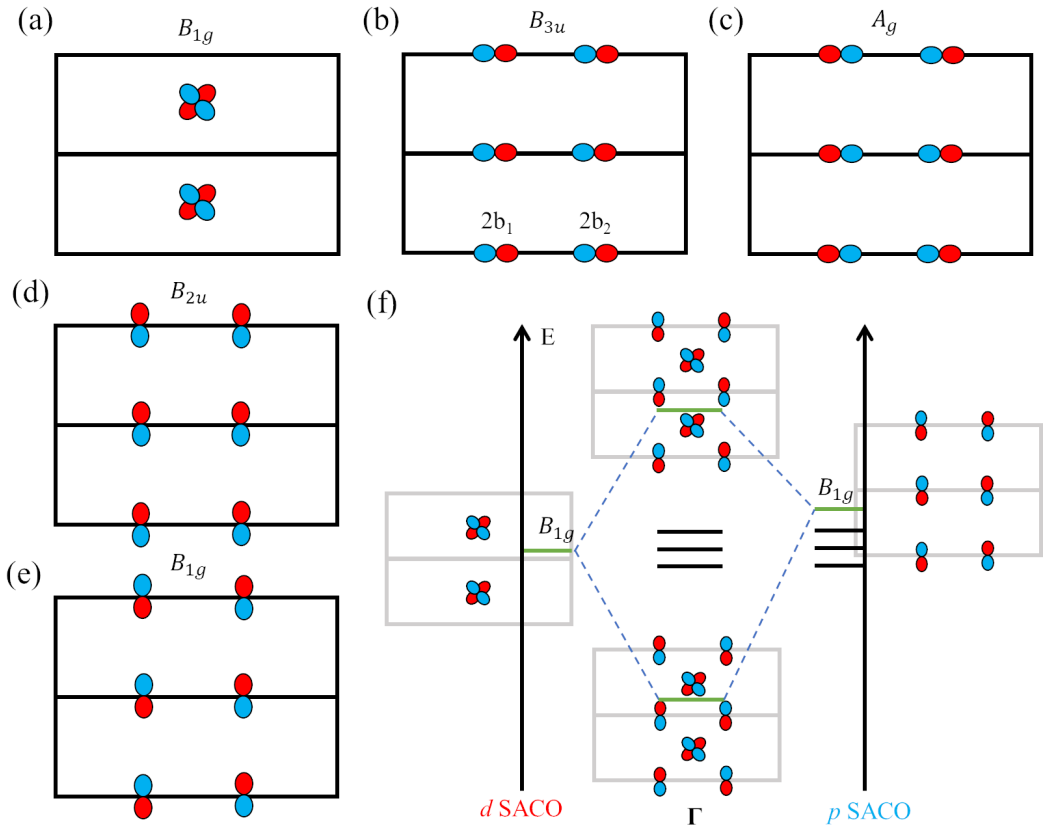


Figure S1: Determination of (a) $d$ SACOs and (b)-(e) $p$ SACOs at Γ. (f) Orbital interaction diagramm at Γ.

After determining the symmetry and energies of both $p$ and $d$ SACOs, the next step is to take $p-d$ hopping into consideration. These $p$ and $d$ SACOs with the same symmetry can interact with each other and form Bloch

states with bonding and anti-bonding nature (both have $B_{1g}$ symmetry). This is illustrated by the $B_{1g}$ $p$ SACOs and $B_{1g}$ $d$ SACOs in Fig. S1(f). The left $p$ SACOs can not interact with $d$ SACO due to different symmetry. Here we consider spinless case and the electronic filling is 4. According to the energy difference between $B_{1g}$ $p$ SACOs and $B_{1g}$ $d$ SACOs, there are two regimes. When the energy difference is much larger than $p-d$ hoppings, we are working at the ionic regime where either $B_{1g}$ $p$ SACOs or $B_{1g}$ $d$ SACOs is totally empty. However, when the energy difference is much smaller than $p-d$ hoppings, there is the co-valency regime as both $B_{1g}$ $p$ SACOs or $B_{1g}$ $d$ SACOs have large occupations and the energy gap between bonding and anti-bonding Bloch states are very large (to ensure a band gap).

To verify that the TB model parameters actually give co-valency regime, here we first map out the energy of $p$ and $d$ SACOs by turning off $p-d$ hoppings ($t_{dp}$ = 0 eV). The orbital-resolved band structure is shown in Fig. S2(a). Obviously, the $B_{1g}$ $d$ SACOs and $B_{1g}$ $p$ SACOs have close energy at both $\Gamma$ and $X$ points. By setting $t_{dp}$ = -1.0 eV, the $B_{1g}$ $d$ SACOs and $B_{1g}$ $p$ SACOs repel each other while the left three $p$ SACOs remain almost the same, as demonstrated in Fig. S2(b).

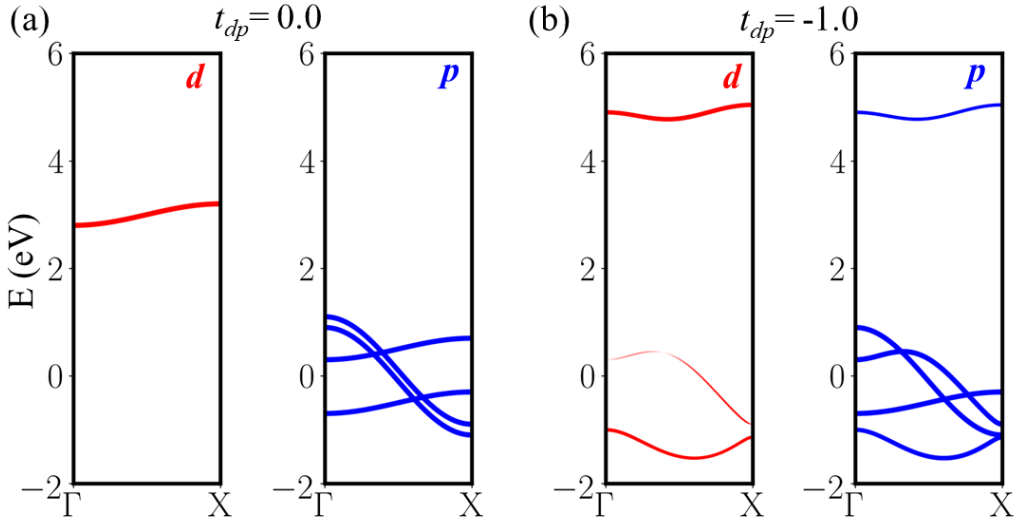


Figure S2: (a) Orbital-resolved band structure at $t_{dp}$ = 0 eV. (b) Orbital-resolved band structure at $t_{dp}$ = -1.0 eV.

### B. Edge states in the 1D TB model

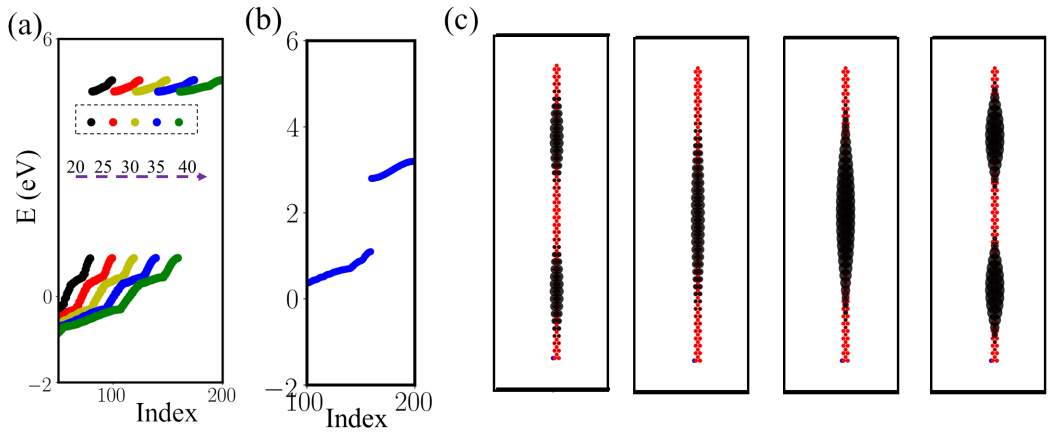


Figure S3: (a) Energy spectrum for open boundary chains with various length. (b) Energy spectrum for a chain of length 40, with $t_{dp}$ = 0 eV. (c) Real-space visualization of four states below and above the bulk gap.

Fig. S3(a) shows the energy spectrum of open boundary chains with different lengths (20, 25, 30, 35 and 40) along $y$ direction. For all the chains, there is an in-gap state marked by the dashed rectangle. Obviously, length

40 is already long enough for the exploration of the in-gap state. The energy spectrum for a chain of length 40 in the AI regime ($t_{dp} = 0$ eV) is also shown in Fig. S3(b). Fig. S3(c) demonstrates the real-space charge distribution of the four states below and above the bulk gap. Obviously, there is no edge state at this regime. .

### C. aBR decomposition of the 60 valance bands

In this section, we show how the 40 valence bands give aBRs decomposition listed in Fig. 3(a). Tab. S1 lists two possible aBRs decomposition for the 60 valence bands of $KCuO_2$. It is noted that below the 40 valance bands shown in Fig. 3(a), there are 20 bands contributed by K's $p$ orbitals and O's $s$ orbital.

Table S1: The aBRs decomposition for the 60 valence bands of $KCuO_2$.

| aBRs ($\rho$@$q$) | Solution 1 | Solution 2 |
|---|---|---|
| $A_1$@$4c$ | 3 | 4 |
| $B_2$@$4c$ | 1 | 2 |
| $B_1$@$4c$ | 2 | 2 |
| $A_2$@$4c$ | 1 | 1 |
| $A'$@$8f$ | 3 | 2 |
| $A''$@$8f$ | 1 | 1 |

According to Tab. I, K's $p$ orbitals and O's $s$ orbital can contribute to $A_1$@$4c$ + $B_2$@$4c$ + $B_1$@$4c$ and $A'$@$8f$ respectively. After deleting the contributions from K's $p$ orbitals and O's $s$ orbital, we have Tab. S2.

Table S2: The aBRs decomposition for the 40 valence bands in Fig. 3(a).

| aBRs ($\rho$@$q$) | Solution 1 | Solution 2 |
|---|---|---|
| $A_1$@$4c$ | 2 | 3 |
| $B_2$@$4c$ | 0 | 1 |
| $B_1$@$4c$ | 1 | 1 |
| $A_2$@$4c$ | 1 | 1 |
| $A'$@$8f$ | 2 | 1 |
| $A''$@$8f$ | 1 | 1 |

For Solution 2, the aBRs $A'$@$8f$ + $A''$@$8f$ must come from O's $p$ orbitals. According to Tab. I, $A''$@$8f$ is contributed by O's $p_z$ orbital, then $A'$@$8f$ means that only $p_x$ or $p_y$ orbital is occupied. Therefore, Solution 2 implies that O atoms are in charge neutral states, which is unreasonable. Therefore, the only reasonable decomposition is given by Solution 1, where the aBRs $2A'$@$8f$ + $A''$@$8f$ suggest that O's $p$ orbitals are fully occupied, leading to $O^{2-}$. At the same time, $2A_1$@$4c$+$B_1$@$4c$+$A_2$@$4c$ comes from Cu's four $d$ orbitals, giving $Cu^{3+}$.

### D. Band structures of cuprates $ACuO_2$ (A=Li, Na, Ru, Cs)

For all the four cuprates, there is an apparent band gap marked by the red arrows, exhibiting a semiconducting phase, as shown in Fig. S4. Similar to the band structure of $KCuO_2$ in Fig. 3(c)-(d), $RuCuO_2$ and $CsCuO_2$ also show some weights of the $B_2$-irrep Cu $d_{yz}$ orbital below the $E_F$ and many weights of the $A'$-irrep/$A''$-irrep O $p_y/p_z$ orbitals above the $E_F$. On the other hand, since $LiCuO_2$ and $NaCuO_2$ have a monoclinic unitcell, they show some weights of the $B_2$-irrep/$B_1$-irrep Cu $d_{yz}/d_{xz}$ orbitals below the $E_F$ and many weights of the $A'$-irrep/$A''$-irrep O $p_x/p_z$ orbitals above the $E_F$. Obviously, the energy bands of these four cuprates both demonstrate an unconventional nature.

### E. The (010) and (1$\bar{1}$0) surface configurations and surface states of $KCuO_2$

When cutting through Cu-O bond/WCCs away from atom, as the (010) surface configuration shown in Fig. S5(a), an obstructed surface state appears in the bulk gap. On contrary, the (1$\bar{1}$0) surface configuration (Fig. S5(c)) not cutting through Cu-O bond/WCCs away from atom doesn't have any obstructed surface state.

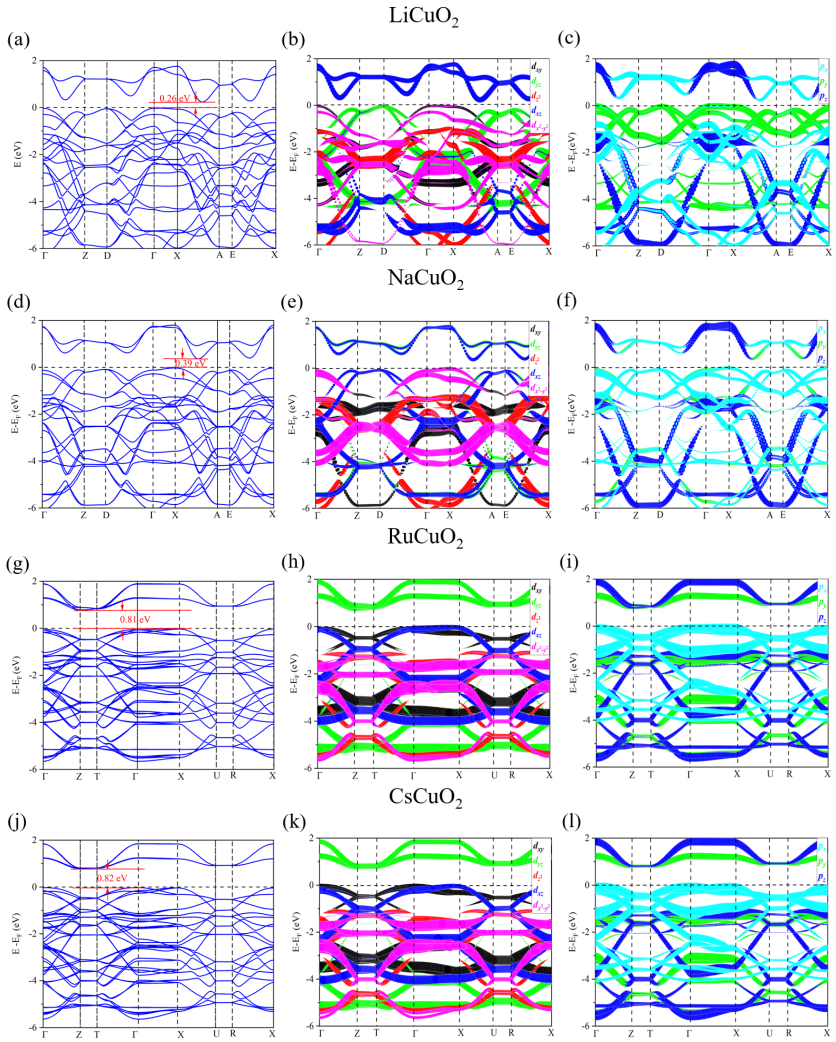


Figure S4: Band structures and orbital-resolved band structures of cuprates (a)-(c) $LiCuO_2$ and (d)-(f) $NaCuO_2$ for a primitive cell, (g)-(i) $RuCuO_2$ and (j)-(l) $CsCuO_2$ for a conventional cell.

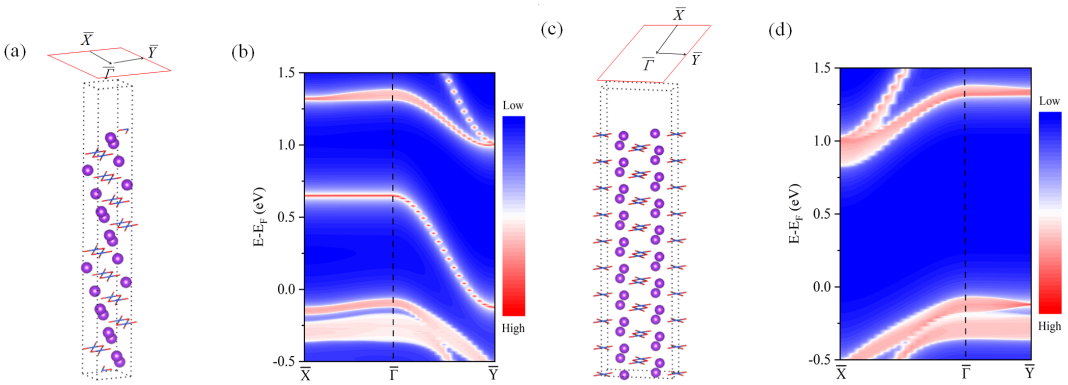


Figure S5: (a) Perspective view of $KCuO_2$ (010) surface. (b) Surface states on (010) surface based on first-principle tight-binding calculation. (c)-(d) are the same as (a)-(b), but for the $(1\bar{1}0)$ surface.

### F. Surface bands and obstructed surface states of cuprates $ACuO_2$ (A=Li, Na, Ru, Cs)

In this section, a series of surface bands of $ACuO_2$ (A=Li, Na, Ru, Cs) are calculated, and the results are depicted in Fig. S6. Obviously, all of them display very similar obstructed surface states just as $KCuO_2$, demonstrating the unconventional nature of electronic states.

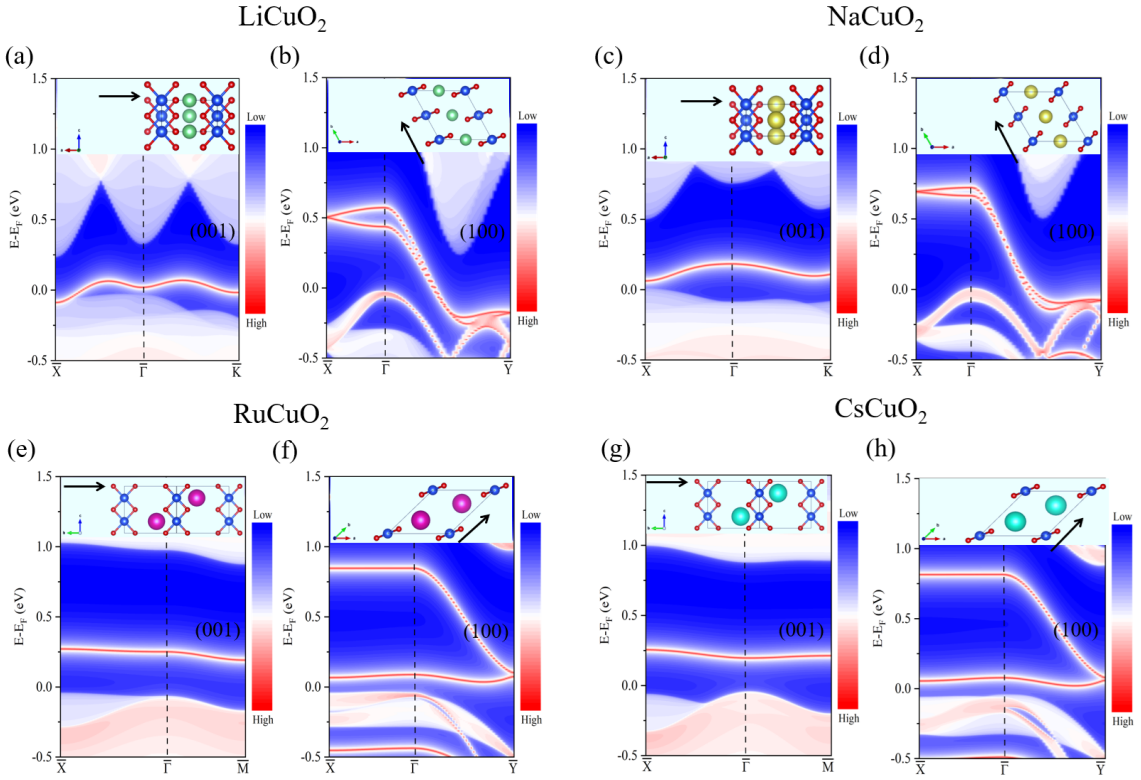


Figure S6: Obstructed surface states on (001) and (100) surfaces for cuprates $ACuO_2$ (A=Li, Na, Ru, Cs).

### G. DFT + U results in $KCuO_2$

In the following, we will show that the unconventional nature in $ACuO_2$ is still preserved even including a hubbard U correction. Taking $KCuO_2$ as a representative, the DFT+U (an 8 eV effective hubbard U parameter is chosen) results are displayed in Fig. S7. Clearly, the dominating effect of hubbard U on electronic states of $KCuO_2$ is to enlarge its band gap (increase by 0.59 eV), but Cu $d_{yz}$/O $p_{y,z}$ orbitals still have substantial weights below/above the $E_F$, as shown in Fig. S7(c)-(d), and the obstructed surface state is also observed in Fig. S7(b).

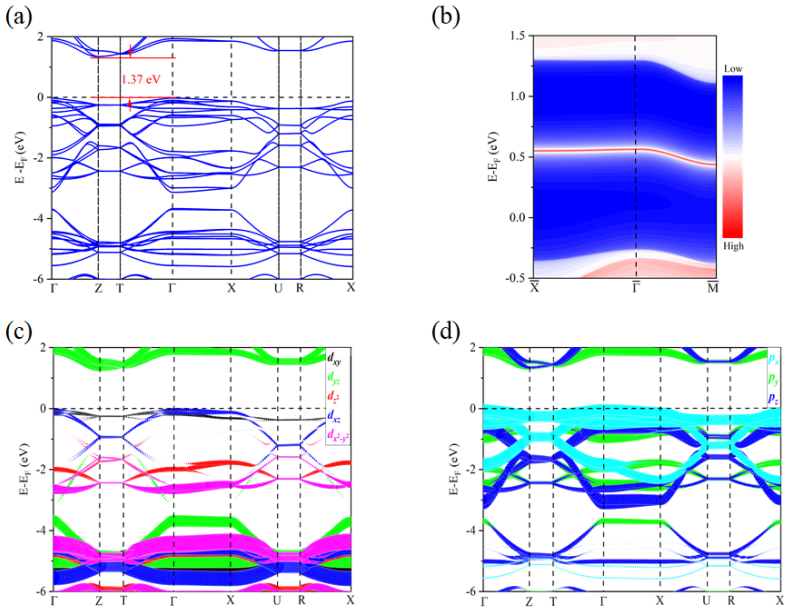


Figure S7: DFT+U results for $KCuO_2$. (a) Band structure and (c)-(d) Orbital-resolved band structures. (b) Surface state on (001) surface based on tight-binding calculation.

These results demonstrate that the unconventionality nature in $ACuO_2$ is very robust against hubbard U.

---

* Electronic address: liubing@wfu.edu.cn
† Electronic address: Zhao.Liu@monash.edu

[1] G. Kresse and J. Furthmüller, *Phys. Rev. B* **54**, 11169 (1996).
[2] S. L. Dudarev, G. A. Botton, S. Y. Savrasov, C. J. Humphreys and A. P. Sutton, *Phys. Rev. B* **57**, 1505 (1998).
[3] J. Heyd, G. E. Scuseria and M. Ernzerhof, *J. Chem. Phys.* **118**, 8207 (2003).
[4] J. Heyd and G. E. Scuseria, *J. Chem. Phys.* **118**, 1187 (2004).
[5] A. A. Mostofi, J. R. Yates, Y.-S. Lee, I. Souza, D. Vanderbilt and N. Marzari, *Comput. Phys. Commun.* **178**, 685 (2008).
[6] Q. Wu, S. Zhang, H.-F. Song, M. Troyer and A. A. Soluyanov, *Comput. Phys. Commun.* **224**, 405 (2018).